14.3 EVOLUTION OF THE HOOK ECHO AND LOW-LEVEL ROTATION IN THE 17 MAY 2000 BRADY, NE SUPERCELL

Michael A. Magsig* and David C. Dowell

Cooperative Institute for Mesoscale Meteorological Studies, Norman, OK

1. Introduction

On 17 May 2000, the Doppler on Wheels (DOW) project intercepted a cluster of supercells, including a tornadic storm near Brady, NE (Fig. 1). The two mobile Doppler radars collected one minute volume scans for extended periods of the tornadic storm's life cycle, which included scans into lower, middle, and upper levels. This unique dataset affords an opportunity to investigate the evolution of a tornadic storm with relatively high temporal and spatial resolution for parts of its lifetime.

Investigation into the evolution of the hook echo and low-level rotation reveals a rather complex evolution of a supercell interacting with numerous small cells and a pre-existing boundary laid out by a neighboring supercell (Fig. 2). The radar data provides evidence that both horizontal advection and precipitation cascade were important in the hook dynamics. The hook echo evolution appears to be influenced by 1) the geometry of the mid-level mesocyclone/mesoanticyclone vortex pair, 2) the intense contortion of the updraft in mid-levels associated with updraft tilting of low-level horizontal vorticity and subsequent stretching of the vertical vorticity in low levels and mid levels, 3) precipitation cascade, and 4) ingesting of hydrometeors by merging cells. The source of rotation in the lowest five hundred meters appears to be associated with the tilting of horizontal vorticity into the vertical and subsequent stretching of the vertical vorticity. The horizontal vorticity is augmented when the inflow of the primary updraft interacts with the boundary laid down by a neighboring supercell.

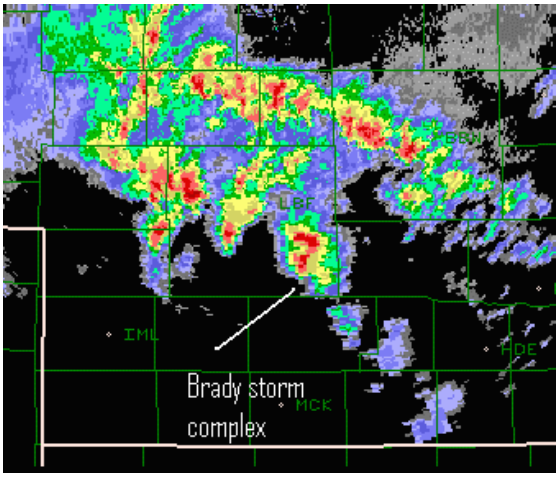

Fig. 1. 2146 UTC radar reflectivity illustrating Brady storm merging with the lead storm in a band of cells that moved north-northwest.

2. Data

Two DOWs, DOW2 and DOW3, collected radar data to obtain dual Doppler coverage of the storms. For a detailed summary of DOW characteristics consult Wurman et al. (1997) and Wurman (2001). Both radars

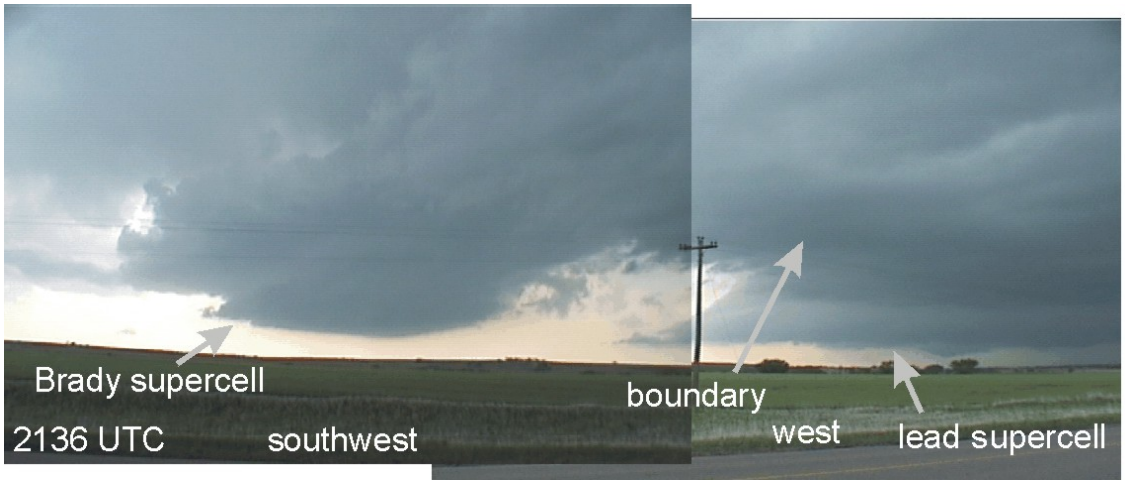

Fig 2. 2136 UTC photos looking SW-W showing the lead supercell, its outflow boundary, and the Brady supercell.

*Corresponding author address: Michael Magsig, CIMMS/WDTB, 3200 Marshall Ave, Norman, OK, 73072, email: Michael.A.Magsig@noaa.gov.

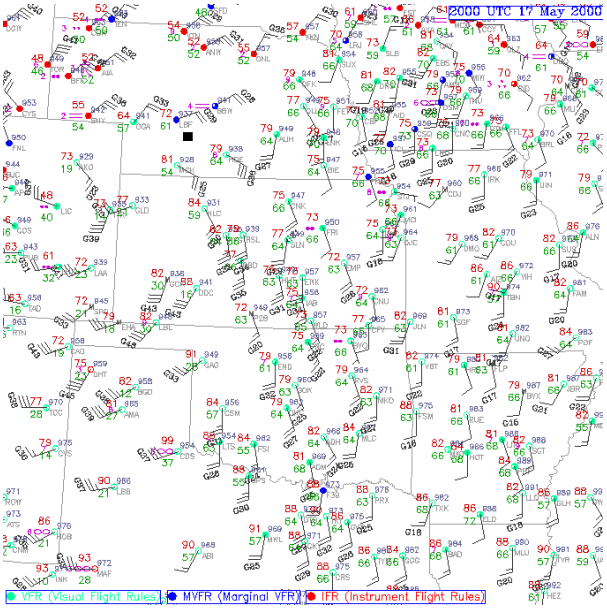

Fig. 3. 20 UTC surface plot with black square indicating the location of the Brady supercell, just to the southeast of LBF.

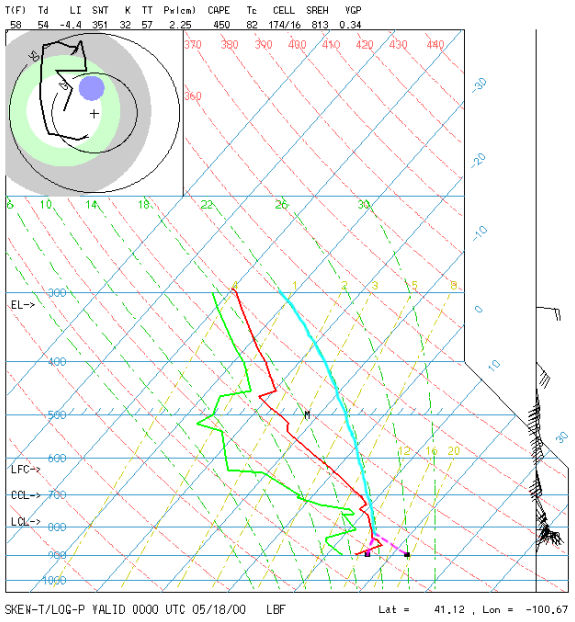

Fig. 4. 0 UTC LBF sounding (parameters on top and side are for unmodified sounding). Annotations illustrate modifying surface with T~72 F and Td~ 61 F.

have beam widths of 1 degrees with 50 m gate spacing, which yields beam diameters of ~ 300 m for a range of 15 km. DOW3 has a Nyquist velocity of 21 m s^{-1}, whereas DOW2 has a Nyquist velocity of 16 m s^{-1}. Display of single Doppler data provided in this paper will be from DOW3. At this time, only two volume scans have been manually unfolded and cleaned up for dual Doppler analysis, so the raw DOW3 velocity data is displayed with no velocity unfolding. Thus velocities will fold over from 21 m s^{-1} to -21 m s^{-1} (red to purple) or from -21 m s^{-1} to 21 m s^{-1} (purple to red) in the radar imagery included. Radar orientation has not been modified, so north is typically pointing to the left.

In the dual Doppler analysis, the data have been manually unfolded and cleaned up using SOLO (Oye et al. 1995). Radar data from both radars have been objectively analyzed to a Cartesian grid using a Cressman interpolation and an influence radius of 750 m. The grid spacing is 250 m in the horizontal and vertical. The currently analyzed data are used to qualitatively diagnose areas of low-level horizontal vorticity, vertical vorticity, and vertical velocity.

3. Environment

The Brady, NE storm formed in a band of convection that moved north-northwest. (Fig. 1). A surface plot from 20 UTC (Fig. 3) shows the storms existed in an area of strong and significantly backed surface winds (30 kts at HDE). Although the nearby LBF surface observation heated up to 77 F with a 61 F dewpoint by 19 UTC, the lower levels cooled by 0 UTC when the LBF sounding was taken (Fig. 4). Modifying the low-level profile with a surface temperature of 72 F and a dewpoint temperature of 61 F yields the parcel profile annotated in Fig. 4. Thus significant instability (LI ~ -10) and vertical wind shear (at least 50 kts of 0-6 km shear) were potentially available for this storm.

4. Anticyclonically Curved Hook

Early in the Brady storm's life (2140 UTC) the geometry of the hook echo appears to be related to the orientation of the vortex pair associated with the mesocyclone and mesoanticyclone aloft (Fig. 5). The vortex pair aloft is consistent with the tilting of ambient vertical wind shear by the updraft early in the storm's evolution. The interesting feature of the hook echo in this early stage is that the hook echo curvature is anticyclonic, a rather unusual configuration. At this time the axis of the hook echo is more correlated with the anticyclonic member of the vortex pair aloft. As the hook echo grows on the rear flank, the tip of the old anticyclonic hook eventually becomes a flair echo on the left flank that "moves" down the left flank, presumably due to the strong propagation of the updraft and hook echo.

Also apparent in Fig 5 is the mature supercell ahead of the Brady storm. The lead supercell laid out an outflow boundary in low levels that is well defined in the DOW data. The speed and motion of the two storms were somewhat similar causing the Brady storm to gradually merge and move along the boundary laid out by the lead storm. The two updrafts and the boundary are clearly visible in the photo displayed in Fig 1.

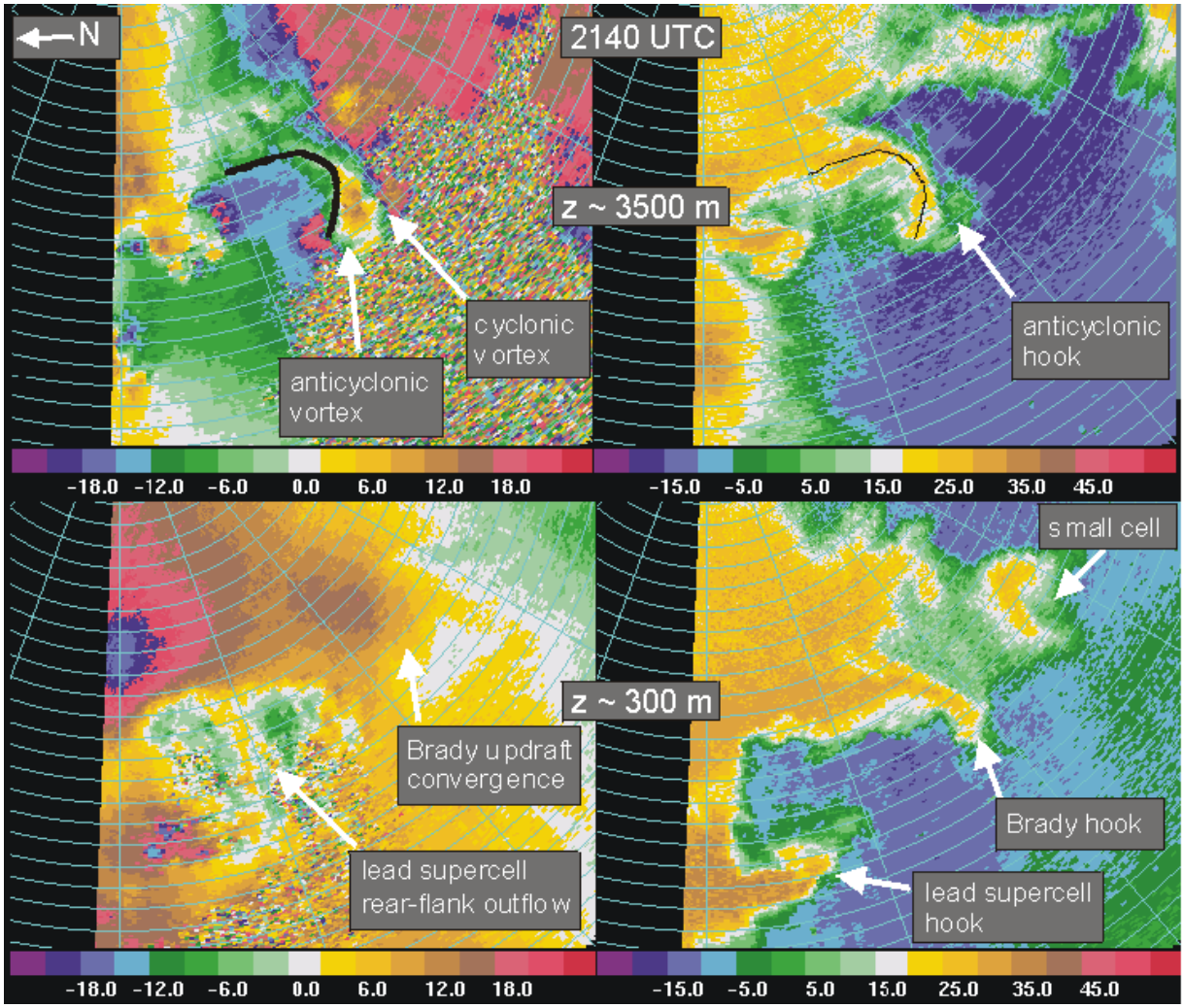

Fig. 5. Doppler velocity (left) and reflectivity (right) for z ~ 3500 m (top) and z ~ 300 m (bottom) at 2140 UTC. Storm is moving north-northwest (right to left). Range rings are every 1 km. Hook echo contains anticyclonic curvature, and the axis of high reflectivities is more correlated with the anticyclonic member of the vortex pair aloft.

5. Hook Echo Streamer

Because the axis of convective initiation was oriented along the cell motion vector, numerous small cells merged with the Brady storm, which affected the precipitation distribution around the updraft. One of the early significant mergers happened shortly after 2140 UTC (Fig. 6). The radar scans in Fig. 5 and Fig. 6 show a small cell was sheared apart is it merged with the Brady updraft. The top of the cell was swept downwind of the main weak echo region due to the strong flow in mid levels on the right flank (see Fig. 5 for strong mid level flow and note velocity unfolding). But in the lowest 3 km, the precipitation was ingested into the convergent flow of the updraft, which subsequently grew upward. Although the axis of the hook is narrow at this time (2 km), the resultant hook echo structure is consistent with Browning's (1964) hook echo streamer, which was also inferred to be contained within updraft. The structure of the hook echo streamer also shows similarities to the streamer in the Apache, OK 3 May 1999 storm investigated in Magsig et al (2002).

Once the hook echo streamer forms, the geometry of the streamer is somewhat similar below 3km. The width is generally ~ 2 km with the high reflectivity axis being about 1 km wide. Above 3 km, the streamer tilts cyclonically with increasing height. Eventually the streamer attaches to the elevated precipitation core aloft forming a bounded weak echo region (BWER, discussed in section 6). Looping through all the tilts of the volume scans further suggests that the hydrometeors ingested into low-level updraft were carried upward cyclonically in intense updrafts where precipitation growth was accelerated.

6. Updraft Pulse

Following the merger of the small cell, a significant updraft pulse developed around 2146 UTC on the rear flank of the storm (Fig. 7). This updraft pulse signaled

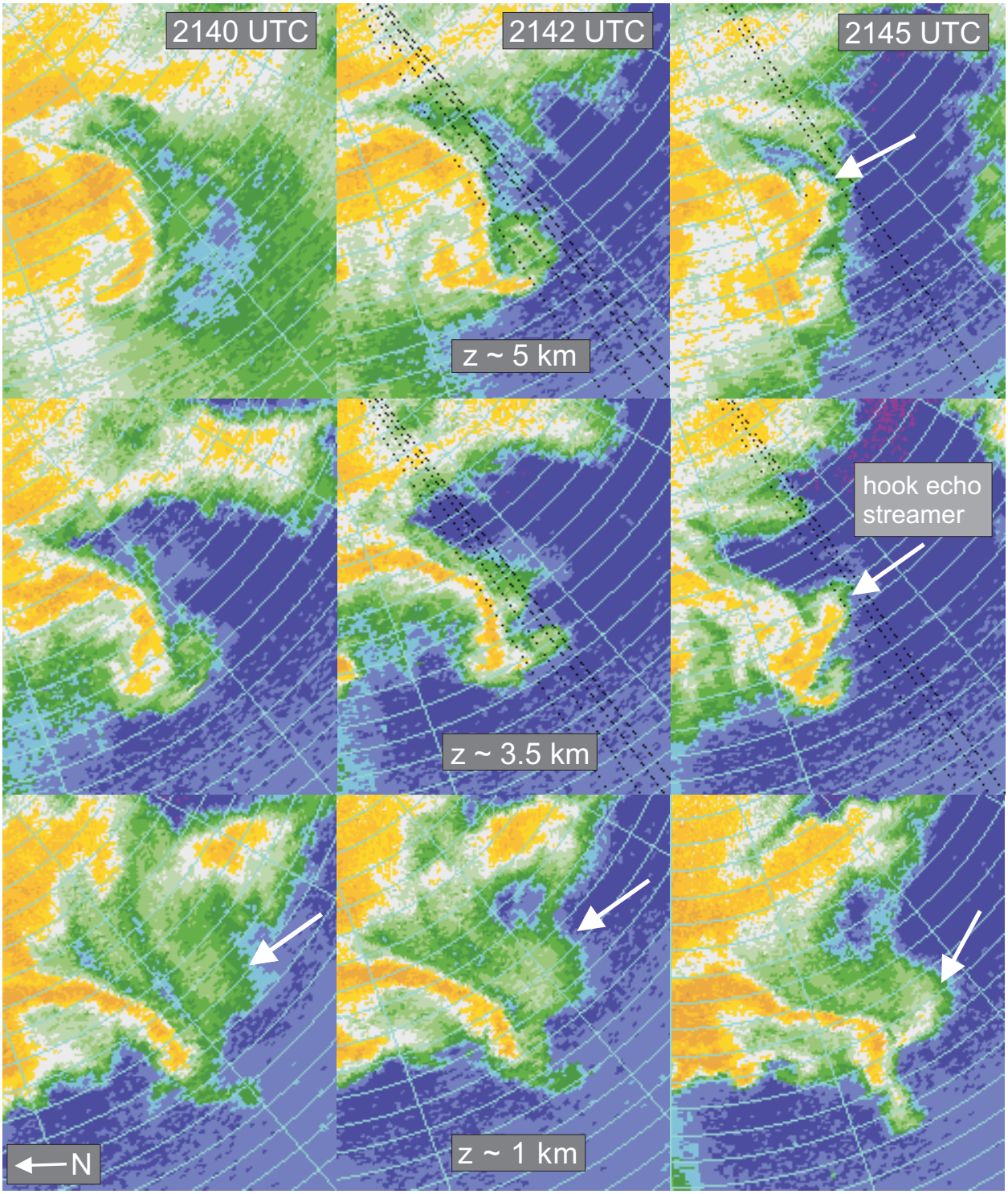

Fig 6. 2140 UTC (left), 2142 UTC (middle), and 2145 (right) reflectivity for z ~ 5 km (top), z ~ 3.5 km (middle), and z ~ 1km (bottom) illustrating the ingesting of hydrometeors into the low-level updraft of the Brady storm leading to the formation of the hook echo streamer.

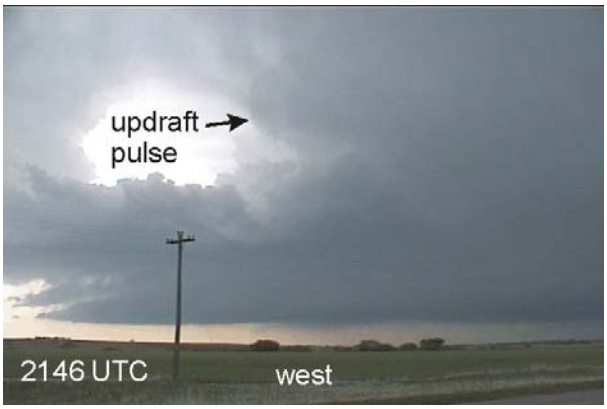

Fig. 7. Picture taken at 2146 UTC looking west at a large updraft pulse in mid levels on the south side of the Brady storm's updraft.

the beginning of a significant transition in storm structure and updraft intensity. Coincident with the updraft pulse is the development of a BWER (Fig. 8) from the hook echo streamer discussed in section 5. Typically the BWER indicates an intense updraft, and the increase in inflow (discussed in section 7) during this time is consistent with a strengthening updraft. Fig. 8 also shows cyclonic rotation existed within the BWER, suggesting updraft rotation. As the BWER developed, the old anticyclonic hook (and vortex pair aloft) began to be "shed" down the left flank.

Following the updraft pulse, a large amount of precipitation was subsequently extruded out the top of the storm on the southwest flank, which descended down the left rear-flank (discussed in section 10). At the time of the appearance of the updraft pulse (2146 UTC), the rear flank outflow of the Brady storm had not yet begun to strongly surge in the lower half of the storm.

7. Low-level Horizontal Vorticity Augmentation

As the Brady storm's inflow rides up and over the boundary laid out by the lead storm, strong horizontal vorticity is generated in the lowest 1 km (Fig. 9). This south-southeastward pointing vorticity shows up well in the dual Doppler analysis at z ~ 500 m AGL (Fig. 10). As this vorticity rich air is ingested into the updraft from the front left flank, it is subsequently tilted upward to produce a new center of rotation in the storm, shifted to the left rear flank.

8. Initial Rear-Flank Outflow Surge and Clear Slot

In between 2147 UTC and 2151 UTC, the rear-flank outflow strongly surges in the lower half of the Brady storm (Fig. 9), severely changing the structure of the hook echo. A narrow jet (~ 1-2 km in width) forms aloft above the surging outflow in concert with the new center of rotation (Fig. 9c), which begins to severely contort the updraft and hook in mid levels, and then subsequently in lower levels. This jet is relatively free of scatterers, and

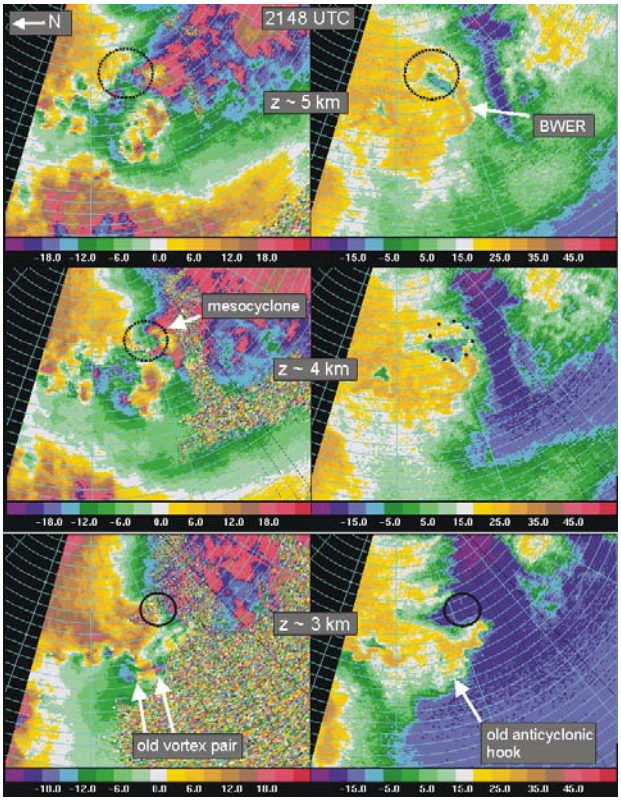

Fig. 8. 2148 UTC velocity (left) and reflectivity (right) for z ~ 5 km (top), z ~ 4 km (middle), and z ~3 km (bottom) illustrating the hook echo streamer forming a BWER. Mesocyclone location is annotated with a solid or dashed circle.

it is consistent with the structure of the clear slot, a wedge of clear air that wraps around the mesocyclone displacing updraft (a feature commonly preceding tornadogenesis). The shift of rotation center from the right flank to the left flank is similar to the evolution observed in the high resolution numerical modeling of the Del City storm in Klemp and Rotunno (1983).

The apparent clear slot is prominent in the lower half of the storm up to about 5 km AGL (Fig 11). There is a very strong correlation of peak radial velocity and a weak echo notch in mid levels from ~ 1-5 km AGL with the clear slot; however, the correlation of velocity peak and reflectivity minimum is much weaker in lower levels (below 1km). These correlations suggest the evolution of the hook echo due to the clear slot in mid levels is strongly affected by horizontal advection, whereas the hook echo structure below cloud base is likely affected by both horizontal advection and vertical precipitation cascade.

9. Mature Rear-Flank Outflow Surge and Clear Slot

As the clear slot wraps around the right flank of the updraft, the peak velocities in the clear slot grow in size and strength giving the appearance of "upscale growth" of the rotation aloft (Fig. 12). The jet of wind in the clear

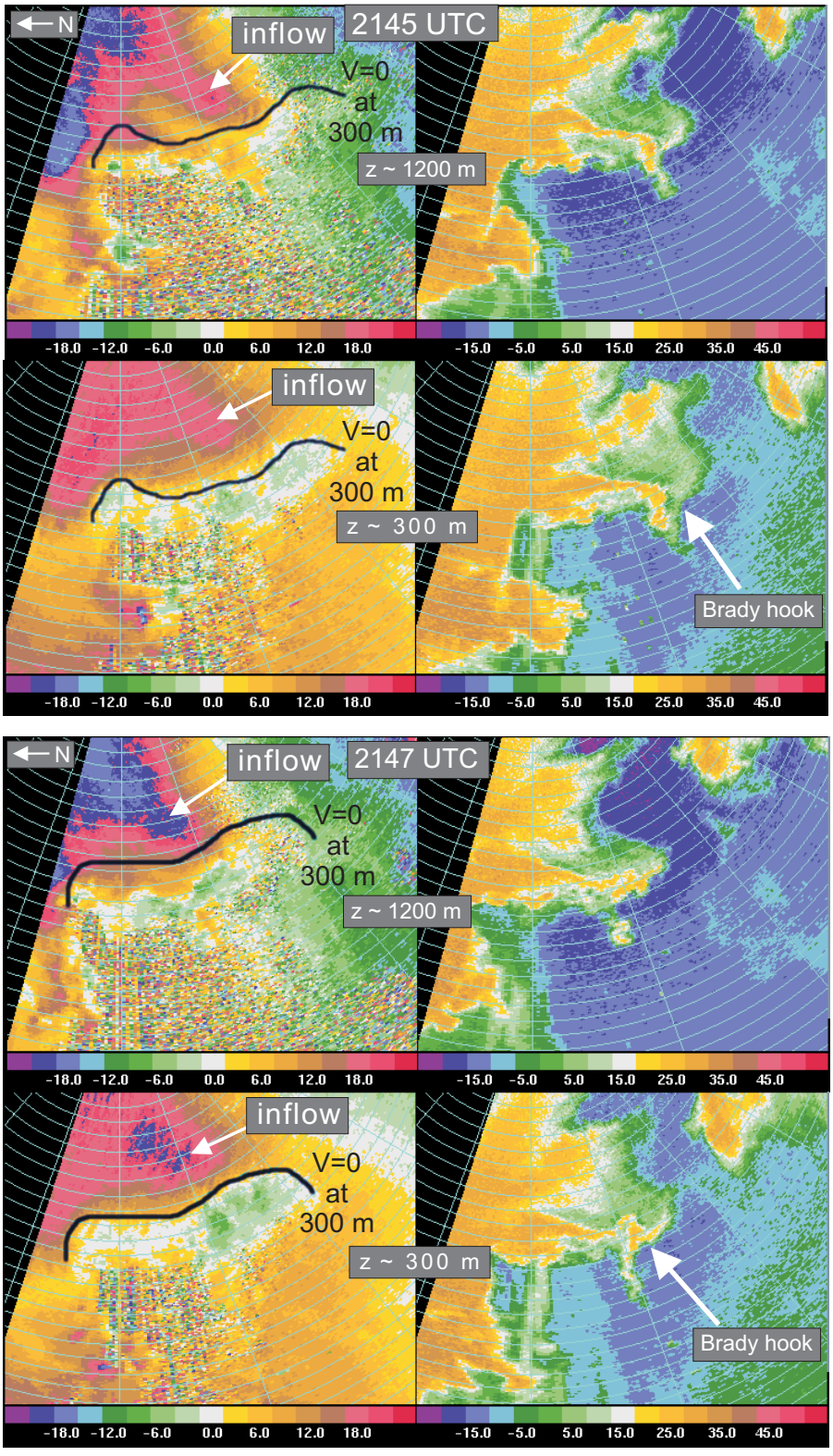

Fig 9 ab. Four panel velocity and reflectivity at 2145 UTC (a: top) and 2147 UTC (b: bottom). Each four panel displays Doppler velocity (left) and reflectivity (right) for z ~ 1200 m and z ~ 300 m. Zero ground-relative isotach along low-level boundary axis at z ~ 300 m is annotated with a black line. Note significant area of enhanced low-level vertical shear is developing as inflow moves over low-level boundary.

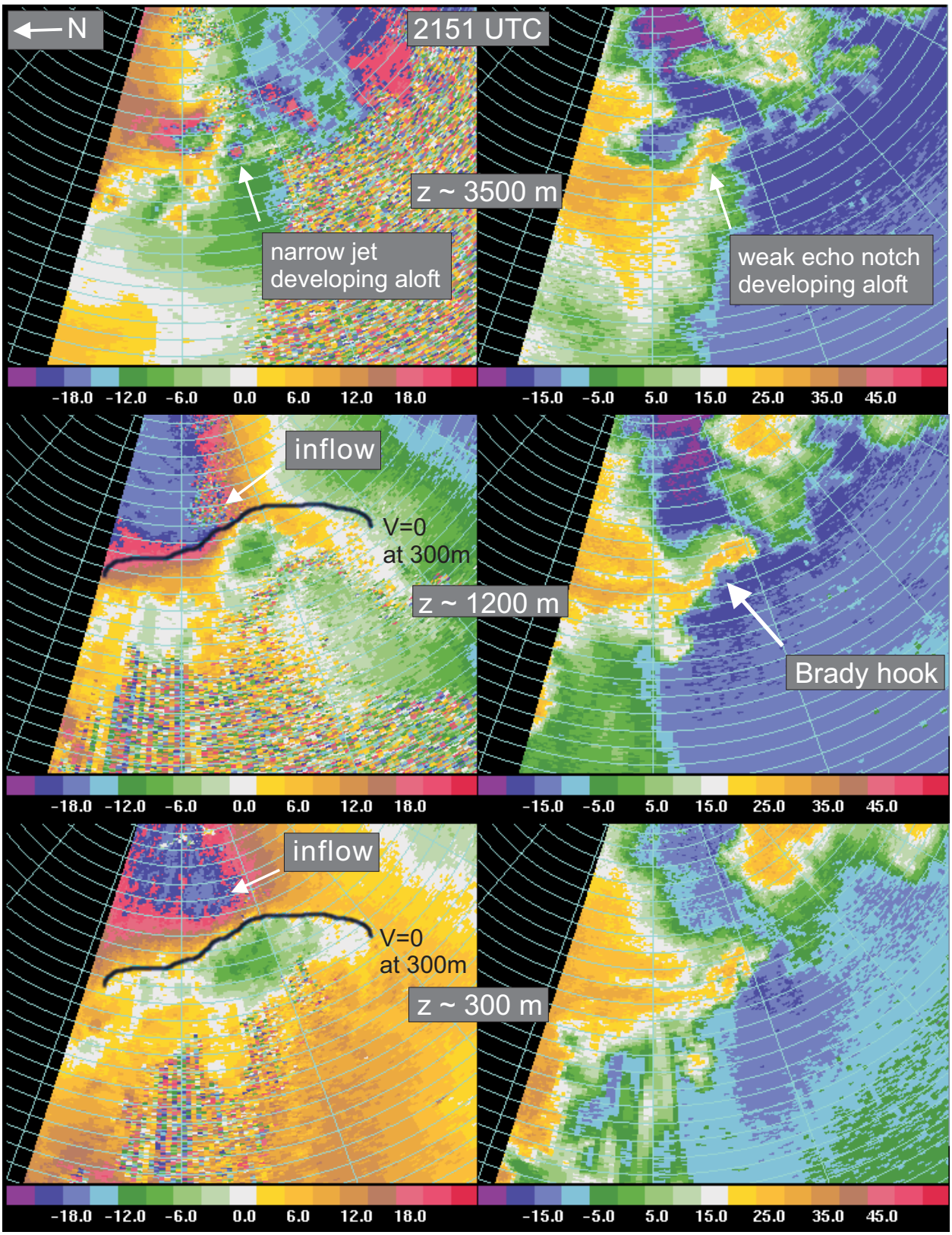

Fig 9c. 2151 UTC velocity (left) and reflectivity (right) for z ~ 3500 m (top), z ~ 1200 m, and z ~ 300 m (bottom). Zero ground-relative isotach along low-level boundary axis at z ~ 300 m is annotated with a black line. Note significant area of enhanced low-level vertical shear as inflow moves over low-level boundary. Also note narrow jet developing aloft.

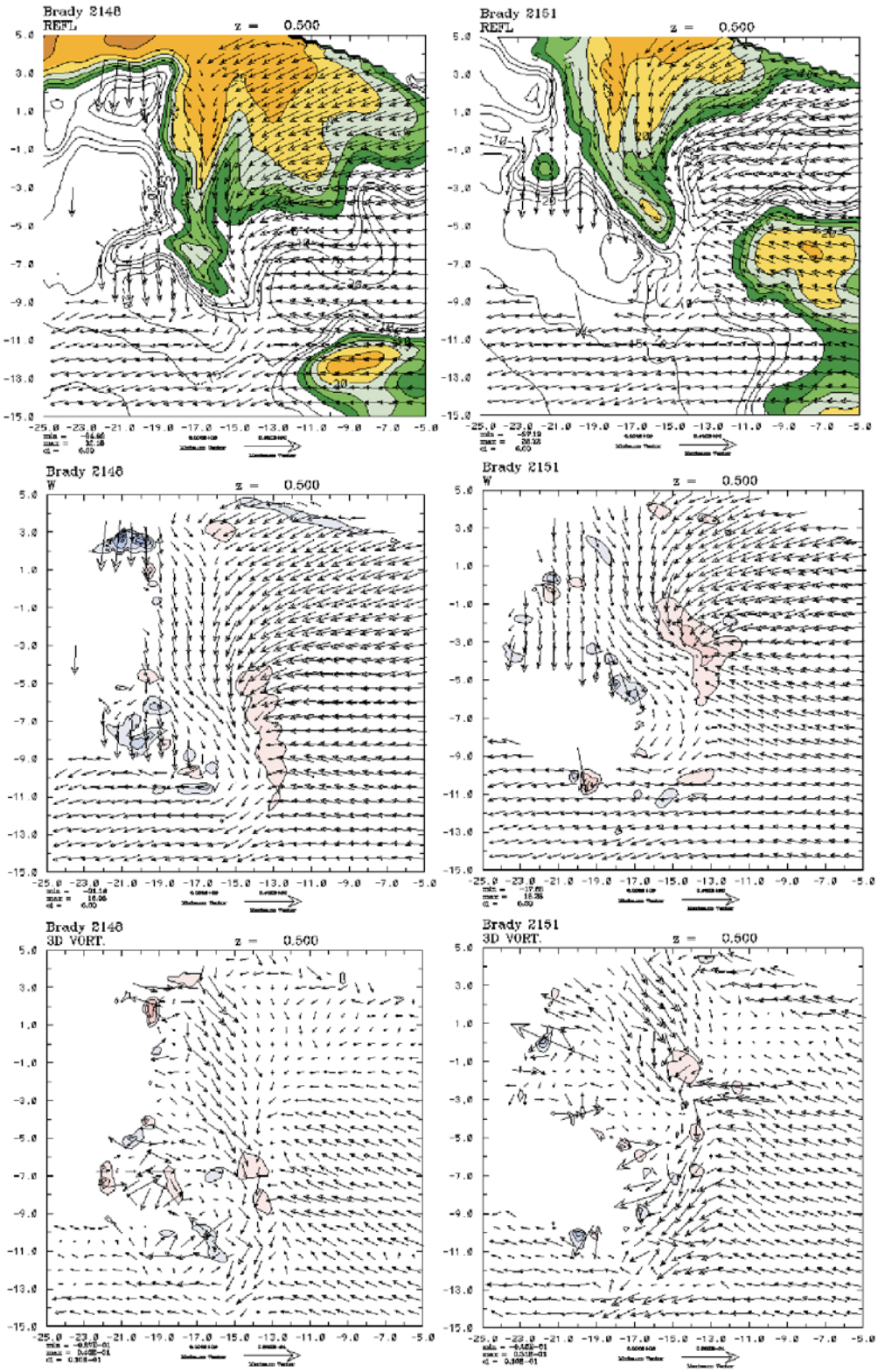

Fig. 10. 2148 UTC (left) and 2151 UTC (right) dual Doppler reflectivity and storm-relative horizontal wind vectors (40 m s-1 reference) [top], vertical velocity (5 m s-1 contours) and storm-relative horizontal wind vectors (40 m s-1 reference) [middle], and horizontal vorticity vectors (0.05 s-1 reference vector) and vertical vorticity (0.01 s-1 contours) [bottom] at z ~ 500 m. Note the southeastward pointing horizontal vorticity vectors strengthen as the inflow moves over the boundary.

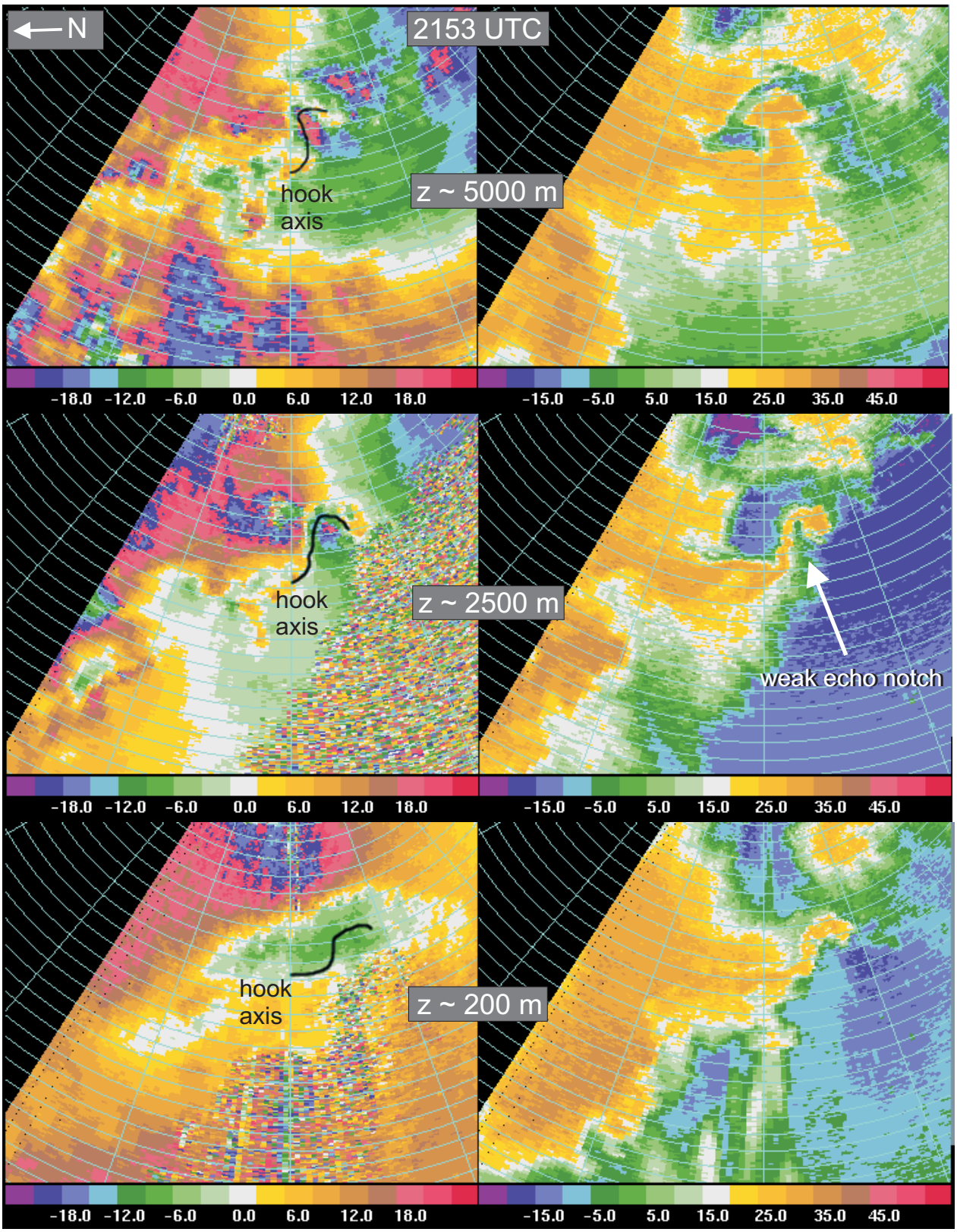

Fig 11. 2153 UTC velocity (left) and reflectivity (right) for z ~ 5000 m (top), z ~ 2500 m (middlle), and z ~ 200 m (bottom). Axis of hook is annotated with the black line. Note the strong correlation at z ~ 2500 m between the velocity peak and the clear slot's reflectivity minimum.

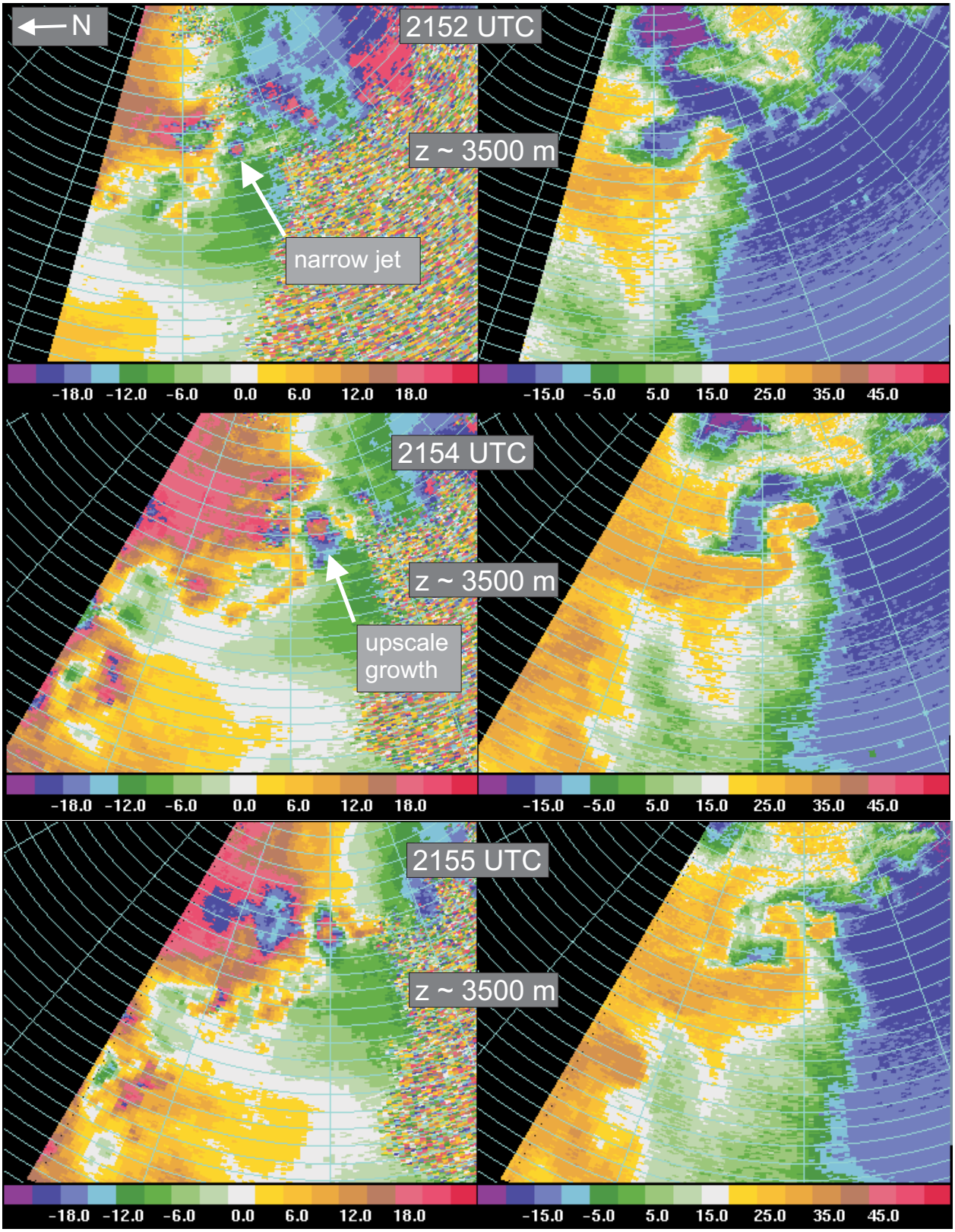

Fig 12. Velocity (left) and reflectivity (right) at z ~ 3500 m and 2152 UTC (top), 2154 UTC (middle), and 2155 UTC (bottom) showing upscale growth of vortex and the clear slot jet severely contorting the hook.

slot so severely contorts the updraft that a near discontinuity forms in the hook, effectively severing the reflectivity streamer of the hook echo. As the nearly separated part of the hook aloft folds back into the clear slot, the echo configuration begins to evolve into a hammerhead appearance, which is a prominent feature up until the tornado forms. A cyclonic-anticyclonic vortex pair straddles the clear slot throughout its depth, but the anticyclonic member is noticeably stronger around 2 km.

10. Hook Widening

After the outflow begins to surge, and the BWER intensifies aloft (2151 UTC), the high reflectivities in the hook substantially increase in size above 4km AGL (see Fig. 11). Above 4 km AGL the width of the high reflectivities in the streamer abruptly increases by a factor of 2-3, to about 2-3 km. Over the subsequent 5-10 minutes there is little change in the width of the lower level max reflectivities, suggesting relatively weak terminal fallspeeds (raindrops) or the presence of updraft slowing the decent of precipitation. One interesting observation is that the tip of the large and fat appendage rotates cyclonically with increasing height toward the center of the BWER (Fig13), further suggesting that a substantial portion of the appendage in mid levels is in updraft at this time.

The widening of the hook through a deep layer occurs closer to 2200 UTC following the descent of a large high reflectivity core that is extruded out the top of the updraft on the left rear flank of the storm (Fig. 13). This core significantly increases the size of the maximum reflectivities in the hook aloft, and then in lower levels. While this significant core is descending, the storm also begins to ingest another cell into the low-level updraft from the southeast (Fig 13). From 2200-2214 UTC, the hook retains a fat hammerhead shape with a large mesocyclone that takes a surprisingly long amount of time to produce a tornado.

11. Tornado

There is a significant gap in radar coverage from 2200-2214 UTC as the DOWs were repositioned. DOW3 collected some volume scans during genesis of the tornado (Fig. 14), though the data set is not as robust as in earlier times. The primary change in storm structure is that the strong rotation extended down to the lowest few hundred meters, whereas earlier the flow contained weaker rotation with convergence. Also, the clear slot filled in with high reflectivities following the descent of the precipitation core down the rear flank, and the low-level velocity peaks became well correlated with the maximum reflectivity peaks. One interesting observation is that there is no stronger low-level rotation in the mesocyclone over that aloft as was found in the Del City storm discussed by Klemp and Rotunno (1983). This interesting observation is consistent with other single Doppler observations of coarser data sets (Magsig and Burgess 1994).

12. Conclusions

Comprehensive data sets with high temporal (1 min volume scans) and spatial resolution (beam widths on the order of 100 m and volume scans in the lowest few hundred meters up to storm top) of tornadic supercells are still quite rare, and much can be learned about the fundamental evolution of the rear-flank outflow and hook echo which can have implications for understanding tornadogenesis. For the Brady storm, the DOWs collected an extensive dataset of a supercell prior to the development of a significant tornado. While the data does not illustrate tornadogenesis in great detail, it does offer insight into the evolution of the hook echo, rear-flank outflow surge, clear slot, and the development of low-level rotation.

One of the important issues discussed by Markowski (2001) in a review of the hook echo is on the nature of the roles of horizontal advection versus precipitation cascade in the evolution of the hook. In this storm, the evolution of the hook echo at times appears to be primarily influenced by horizontal advection from cloud base to mid levels (~ 1-5 km), relating to the initial mesocyclone/mesoanticyclone vortex pair aloft and the development of a clear slot and rear-flank outflow surge. Precipitation cascade appears to be more consistently significant in upper levels of the storm as well as below cloud base, though descent of large reflectivity cores can at times affect all levels of the hook echo. In addition to these factors, the ingesting of hydrometeors by relatively weak neighboring cells was found to significantly impact the structure of the hook echo.

Hook echoes have long been associated with downdrafts (Markowski 2001); however, significant parts of the hook echo throughout the depth of the storm appear to be located in updraft. As further refinements in the dual Doppler analysis are made for this case, the relationship between updraft, downdraft, and hook echo will be explored in more detail.

One of the interesting facets of this event is the evolution of the augmented low-level horizontal vorticity along a boundary laid out by an existing storm. The horizontal vorticity appears to have been significantly increased as the accelerated inflow from the Brady storm moved over the pre-existing boundary laid out by a lead supercell (Fig. 15).

Another interesting observation in this case is that the rear-flank outflow surge and clear slot development appear to be tied to the updraft tilting of low-level horizontal vorticity, which results in the development of low-level rotation (lowest five hundred meters) and mid-level rotation. While E. N. Rasmussen (personal communication) has found “blobs” of precipitation to be associated with the development of low-level rotation in some storms, this case does not appear to have the same type of mechanism. While the filling in of the clear slot by a large descending blob could conceivably be important in the development of the tornado, the initial low-level rotation preceded the descent of the blob.

While there are some similarities in the development of rotation in this storm with classic models

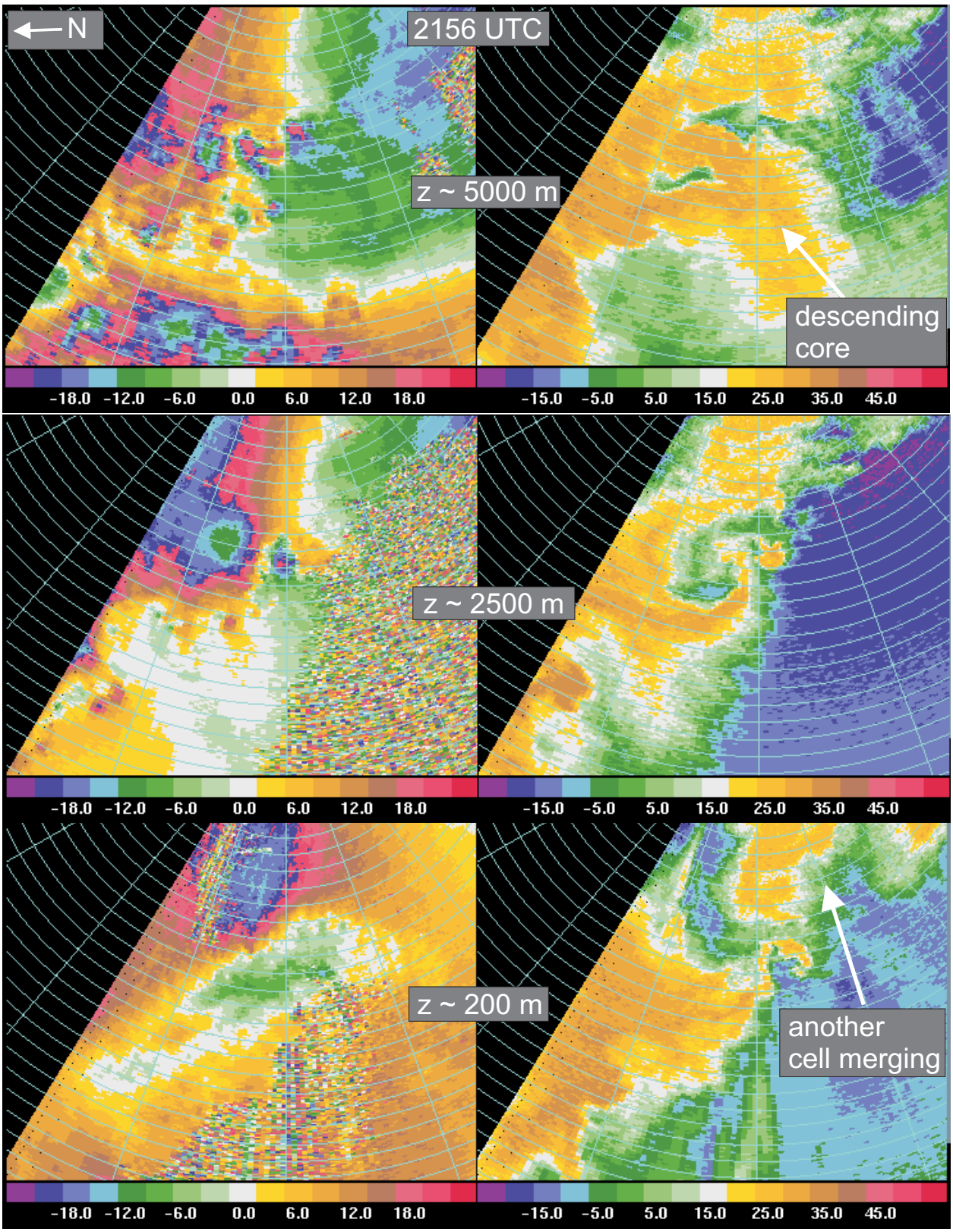

Fig 13. 2156 UTC velocity (left) and reflectivity (right) for z ~ 5000 m (top), z ~ 2500 m (middle), and z ~ 200 m (bottom). Note the reflectivity in the hook at z ~ 5000 m is beginning to widen as a massive core descends down the left-rear flank from aloft. Also note another cell beginning to merge with the updraft.

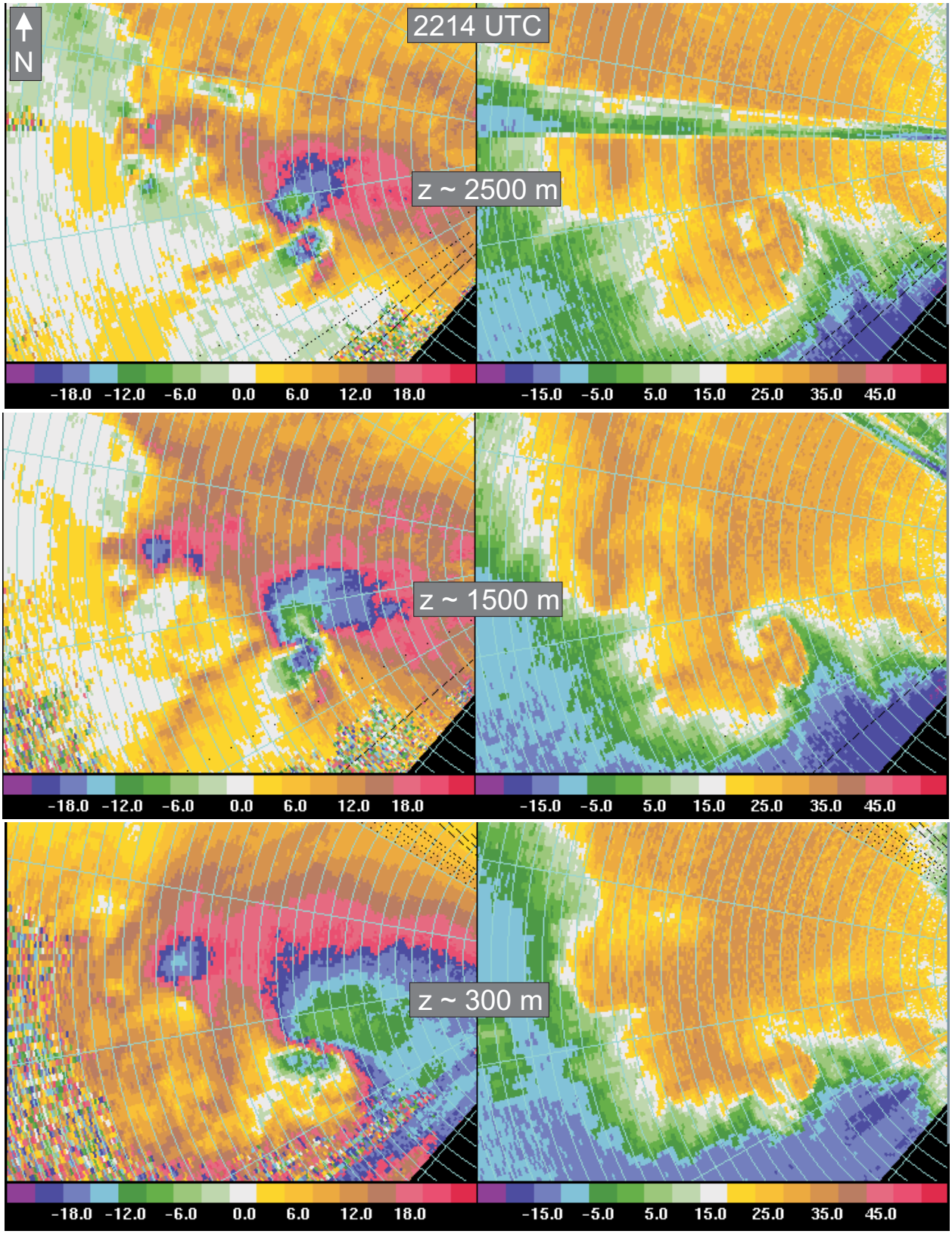

Fig 14. 2214 UTC velocity (left) and reflectivity (right) for z ~ 2500 m (top), z ~ 1500 m (middle), and z ~ 300 m (bottom) during tornadogenesis. Note the radar has turned, and north is to the top. By 2214 UTC a strong circulation has developed down to z ~ 300 m, and a localized vortex is detected at z ~ 1500 m.

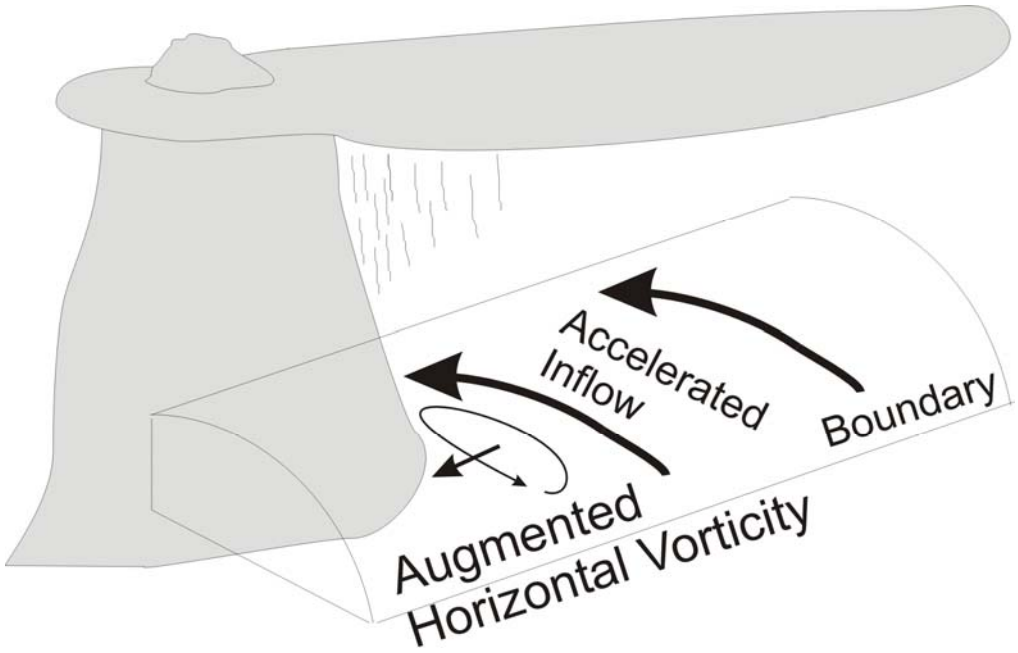

Fig. 15. Conceptual model of low-level horizontal vorticity amplification through accelerated inflow moving over a low-level boundary left over from a nearby supercell.

(Klemp and Rotunno 1983), there is at least one notable difference. The rotation near the ground does not exceed that aloft prior to the tornado following the surging rear-flank gust front (i.e. no occlusion downdraft mechanism). This has been noted in other single Doppler studies (Magsig and Burgess 1994), though the frequency of the occlusion downdraft mechanism has yet to be fully explored.

The complex evolution of the Brady supercell captured by the high resolution radar data sets offers a unique perspective on tornado forecasting and warning. Operational radar data sets do not have the temporal nor spatial resolution to begin to capture the evolution of the important small scale features illustrated in this case. Rather than processes being made clear, the high resolution data sets are somewhat challenging to understand, and they tend to raise more questions than provide answers. This suggests there are significant advances in knowledge that can be obtained by investing in higher resolution data sets and further research and development. The complexities of this type of event are also good to incorporate into training of operational warning forecasters, to expose forecasters to the large degree of uncertainty inherent in using operational radars for tornado warning operations.

13. Acknowledgements

DOW radar data were provided by Josh Wurman, David Dowell, Bill Martin, MyShelle Bryant, Curtis Alexander, Yvette Richardson, Steve McDonald and Paul Ritter. Surface and upper air images are from the case selection kit (http://locust.mmm.ucar.edu/case-selection/) maintained by the Precipitation Diagnostics Group of the Mesoscale and Microscale Meteorology Division of NCAR. This work was supported under Cooperative Agreement NA17RJ1227 of the NOAA-University of Oklahoma/Cooperative Institute for Mesoscale Meteorological Studies.

14. References

Browning, K. A., 1965: Some inferences about the updraft within a severe local storm. *J. Atmos. Sci.,* **22**, 669-677.

Klemp, J. B., and R. Rotunno,. 1983: A Study of the Tornadic Region within a Supercell Thunderstorm. *Journal of the Atmospheric Sciences*: Vol. 40, No. 2, pp. 359–377.

Magsig, M. A., D. W. Burgess, D. C. Dowell, Y. P. Richardson, and J. M. Wurman, 2002, The structure and evolution of hook echoes during tornadogenesis as revealed by high resolution radar data. Preprints, *21st Conf. on Severe. Local Storms*, San Antonio, TX, Amer. Meteor. Soc. 12-16 Aug, 2002.

Magsig, M. A. and D. W. Burgess, 1994, A vorticity and divergence analysis relating to tornadogenesis as seen by a WSR-88D radar. Preprints, *18th Conf. on Severe. Local Storms*, Amer. Meteor. Soc., 19-23 Feb., 1996, 418-422.

Markowski, P. M., 2001: Hook echoes and rear-flank downdrafts: a review. *Mon. Wea. Rev.*, **130**, 852-876.

Oye, R., C. Mueller, and S. Smith, 1995: Software for radar translation, visualization, editing, and interpolation. Preprints, *27th Conf. on Radar Meteorology,* Vail, CO, Amer. Meteor. Soc.,359–361.

Wurman, J., J. M. Straka, E. N. Rasmussen, M. Randall, A. Zahrai, 1997: Design and deployment of a portable, pencil-beam, pulsed, 3-cm Doppler radar. *J. Atmos. and Oceanic Technol.*, **14**, 1502–1512.

Wurman, J., 2001: The DOW mobile multiple-Doppler network. *Preprints,30th Conf. on Radar Meteorology*, Munich, Germany, 95-97.